Preparation and Properties of Spinel $LiMn_{1.90}$ $Ni_{0.05}$ $Cu_{0.05}$ O_4

Yonggen Li[1], Yin Liu[2, *]

[1]College of Biology and Chemistry, Pu'er College, Pu'er, Yunnan, 665000, China
[2]Yunnan Provincial Hydrology and Water Resources Bureau, Kunming Branch, Kunming, Yunnan, 650500, China
[*] Corresponding author

Abstract: Spinel $LiMn_2O_4$ and $LiMn_{1.90}Ni_{0.05}$ $Cu_{0.05}O_4$ cathode materials were synthesized by a simple solution combustion method. The structure, morphology and properties of the two samples were characterized by X-ray diffraction (XRD), scanning electron microscopy (SEM), battery test system and electrochemical workstation. The results show that the two samples are spinel lithium manganate structure, which can be indexed as Fd3m space group. Ni Cu co doping effectively reduces the particle size and agglomeration, improves the crystallinity of the materials, and makes $LiMn_{1.90}Ni_{0.05}Cu_{0.05}O_4$ samples show good crystal structure stability and magnification properties. The capacity retention rates of 64.53%,79.52%and 69.47%were obtained after 1000 cycles at current densities of 1 C,5 C and 10 C,respectively, which were higher than 43.75%,55.74%and 44.38%of the corresponding undoped $LiMn_2O_4$ samples.

Keywords: Spinel-type lithium manganese dioxide; Solution combustion method; Nickel-copper co-doping; Anode materials.

1. Introduction

Lithium ion batteries have been widely used in small digital electronic products, electric vehicles, aerospace and other fields due to their large energy density and high output voltage [1-2] . The electrochemical performance and energy density of lithium-ion batteries are mainly determined by the properties of cathode materials. At present, the more mature commercial cathode material for lithium-ion batteries is $LiCoO_2$. Due to the low reserves and toxicity of Co resources, it cannot meet the market competition and large-scale commercial production [3-4] . Compared with $LiCoO_2$, spinel $LiMn_2O_4$ has the advantages of rich resources and environmental friendliness. It is considered that it can replace $LiCoO_2$ as the ideal cathode material [4-5] for lithium-ion power batteries. However, the loss of manganese [6-7] caused by lattice distortion and disproportionation reaction caused by Jahn Teller effect, as well as the decomposition of electrolyte at high temperature and the existence of oxygen defects destroy the stability of crystal structure [8-9] , resulting in the capacity attenuation of spinel $LiMn_2O_4$ at high temperature and high magnification.

At present, the main methods to improve the electrochemical characteristics of spinel $LiMn_2O_4$ are element doping and surface coating. The commonly used coating agents are Al_2O_3 , V_2O_5 , Mn_2O_3 , La_2O_3 and ZnO [10] . Low valence cations such as Li^+, Na^+, Cu^{2+}, Ni^{2+}, Mg^{2+}, Zn^{2+}, Co^{3+}, Cr^{3+}, Al^{3+}, etc. are usually used to improve the average valence state and lattice stability of Mn [11-12] . Zhu Jinyu [13] et al. synthesized spinel $LiNi_{0.08}Cu_{0.05}Mn_{1.87}O_4$ cathode material by flameless combustion method. The results show that Ni Cu co doping reduces the lattice constant of the sample, shrinks the cell, and shows smaller particle size, between 60-100 nm, which effectively improves the crystallinity and lattice stability of the material. The first specific capacity of $LiNi_{0.08}Cu_{0.05}Mn_{1.87}O_4$ sample is 104.7 $mAhg^{-1}$ when charged and discharged at room temperature of 1 C and 3.6-4.5 V, and the capacity retention rate after 200 cycles is 81.38%, which is higher than 65.16% of the undoped $LiMn_2O_4$ sample. Its high temperature performance and high magnification performance have also been significantly improved. After 1000 cycles at 5 C and 200 cycles at 55 ℃ (1 C), the capacity retention rates are 68.23% and 56.23%, respectively, which are superior to the undoped $LiMn_2O_4$ samples. Zhang Chunling [14] et al. synthesized 5V spinel $LiMn_{1.5}Ni_{0.5-x}Cu_xO_4$ cathode material by liquid coprecipitation method. When charging and discharging at a current density of 2.0 mA cm^{-2} and a voltage of 3.0-5.0 V, its first discharge capacity can be as high as 129.4 $mAhg^{-1}$, and its capacity retention rate after 200 cycles is 67%.

In this paper, a simple solution combustion method is used to make Cu and Ni uniformly doped into the spinel phase of $LiMn_2O_4$ to replace the active Mn on the 16d position of octahedron, and generate Ni-O bond (1.915 A) and Cu-O bond (1.95 A) shorter than Mn-O bond (2.16 A), The influence of Ni Cu co doping on spinel $LiMn_2O_4$ was systematically discussed through structural analysis and performance test.

2. Experimental Methods

2.1. Preparation of materials

Taking Mn $(CH_3COO)_2 \cdot 4H_2O$ (AR), $LiNO_3$ (AR), Ni $(CH_3COO)_2 \cdot 4H_2O$ (AR) and Cu (NO_4 After weighing, put it into the crucible, add 3.5 mL of HNO_3 (AR) as the solvent, Dissolve at 80 ℃ to form solution. The solution is placed in a muffle furnace with a preset temperature of 300 ℃ and calcined for 3 hours to obtain the product as shown in Figure 1. After it is ground into powder, it is further placed in a muffle furnace with a preset temperature of 600 ℃ and calcined for 6 hours to obtain the target product.

2.2. Assembly of CR2030 battery

The prepared $LiMn_2O_4$ and $LiMn_{1.90}Ni_{0.05}Cu_{0.05}O_4$ powders are weighed accurately with carbon black and polyvinylidene fluoride (PVDF. Evenly apply the slurry on the collector aluminum foil, vacuum dry it for more than 12 hours, and cut it into 16 mm diameter discs. This disc is the cathode material, which is assembled with the cathode material lithium metal sheet, polypropylene diaphragm, $LiPF_6$ electrolyte in the high-purity Ar glove box (super1220/750) to form the CR2032 button lithium ion battery.

2.3. Structural characterization and performance testing

X-ray diffractometer (XRD, D8 ADVANCE, Bruker Company) to detect the phase structure of the powder; Scanning electron microscope (SEM, NOVANANOSEM 450, FEI Company of the United States) was used to observe the micro morphology and size of the samples; The LAND constant current test system (Wuhan Jinnuo Electronics Co., Ltd.) tests the cycle performance and magnification performance of the assembled battery, with a voltage range of 3.0~4.5 V; The electrochemical workstation (CHI 660E model, Shanghai Chenhua Instrument Co., Ltd.) carries out cyclic voltammetry (CV, voltage 3.6~4.5 V) and electrochemical impedance (EIS, frequency 0.1 Hz~100 kHz) tests.

3. Results and Discussion

3.1. Characterization and analysis of macroscopic morphology, the

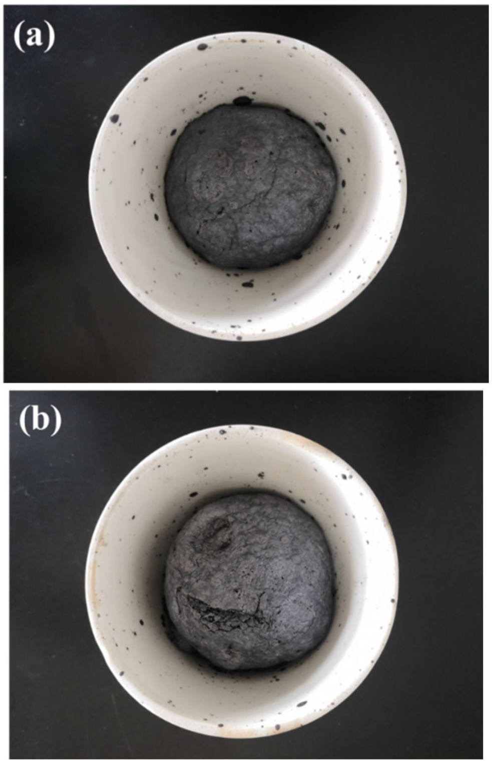

Fig. 1 Macro view of (a) $LiMn_2O_4$ and (b) $LiMn_{1.90}Ni_{0.05}Cu_{0.05}O_4$

Fig. 1 Apparent morphology of (a) $LiMn_2O_4$ and (b) $LiMn_{1.90}Ni_{0.05}Cu_{0.05}O_4$

Figure 1 (a) and (b) are the macroscopic views of $LiMn_2O_4$ and $LiMn_{1.90}Ni_{0.05}Cu_{0.05}O_4$ obtained after the solution was calcined in a muffle furnace with a preset temperature of 300 °C for 3 h. As shown in the figure, the macroscopic appearance of the two samples is very similar, black, slightly fluffy, and the volume accounts for about one-third of the entire 300 mL porcelain crucible. This is because CO_2 generated during combustion and NO_2 and O_2 generated from decomposition of solvent HNO_3 promote the expansion of product volume.

3.2. X-ray diffraction (XRD) analysis

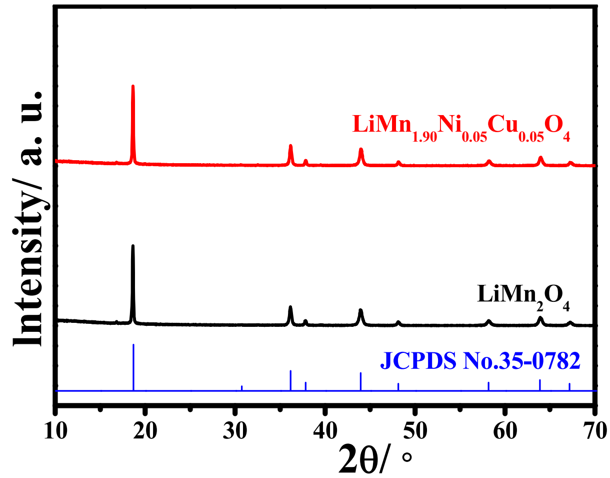

Figure 2. XRD Spectra of $LiMn_2O_4$ and $LiMn_{1.90}Ni_{0.05}Cu_{0.05}O_4$

Figure 2. XRD spectra of $LiMn_2O_4$ and (b) $LiMn_{1.90}Ni_{0.05}Cu_{0.05}O_4$

As shown in Figure 2, the XRD spectra of the synthetic samples $LiMn_2O_4$ and $LiMn_{1.90}Ni_{0.05}Cu_{0.05}O_4$, the diffraction peaks of both samples are consistent with the standard spinel $LiMn_2O_4$ (JCPDS, NO.35-0.82), which is the structure of the Fd3m space group. Li occupies the position 8a of the tetrahedron, and Mn occupies the position 16d of the octahedron. At 2 θ = No redundant diffraction peak was detected at 30.7 °, indicating that Mn [15] on octahedron (16d) was substituted by Ni Cu co doping. The lattice parameters of $LiMn_2O_4$)and LiMn [16] $Ni_{0.05}Cu_{0.05}O_4$.

3.3. Scanning electron microscope (SEM) analysis

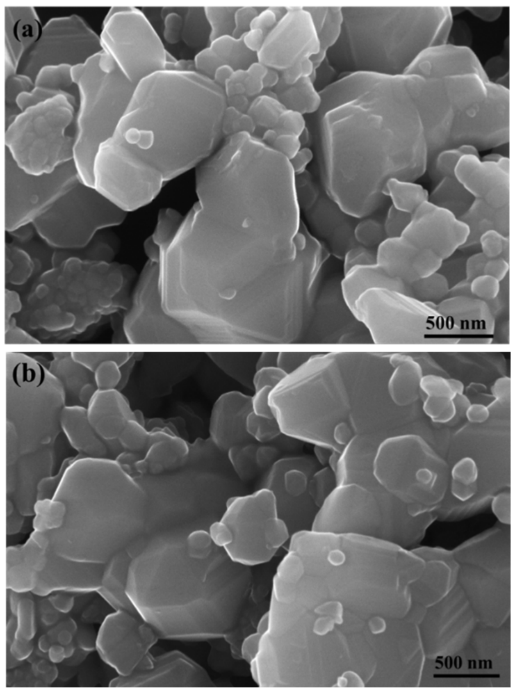

Figure 3. SEM Diagram of (a) $LiMn_2O_4$ and (b) $LiMn_{1.90}Ni_{0.05}Cu_{0.05}O_4$

Figure 3. SEM spectra of $LiMn_2O_4$ and (b) $LiMn_{1.90}Ni_{0.05}Cu_{0.05}O_4$

Fig. 3 (a) and (b) are SEM images of $LiMn_2O_4$ and $LiMn_{1.90}Ni_{0.05}Cu_{0.05}O_4$, respectively. As shown in the figure, fine particles agglomerate in both sample particles, and the particle size difference is large. Small particles can be detected at about 200 nm, while large particles develop to 500 nm~1 μ M. But in general, the overall particle size and agglomeration of $LiMn_{1.90}Ni_{0.05}Cu_{0.05}O_4$ are slightly smaller than that of $LiMn_2O_4$, and the edges are more clear and distinct, which means that Ni Cu co doping helps to improve the crystallinity of materials.

3.4. Cyclic performance testing

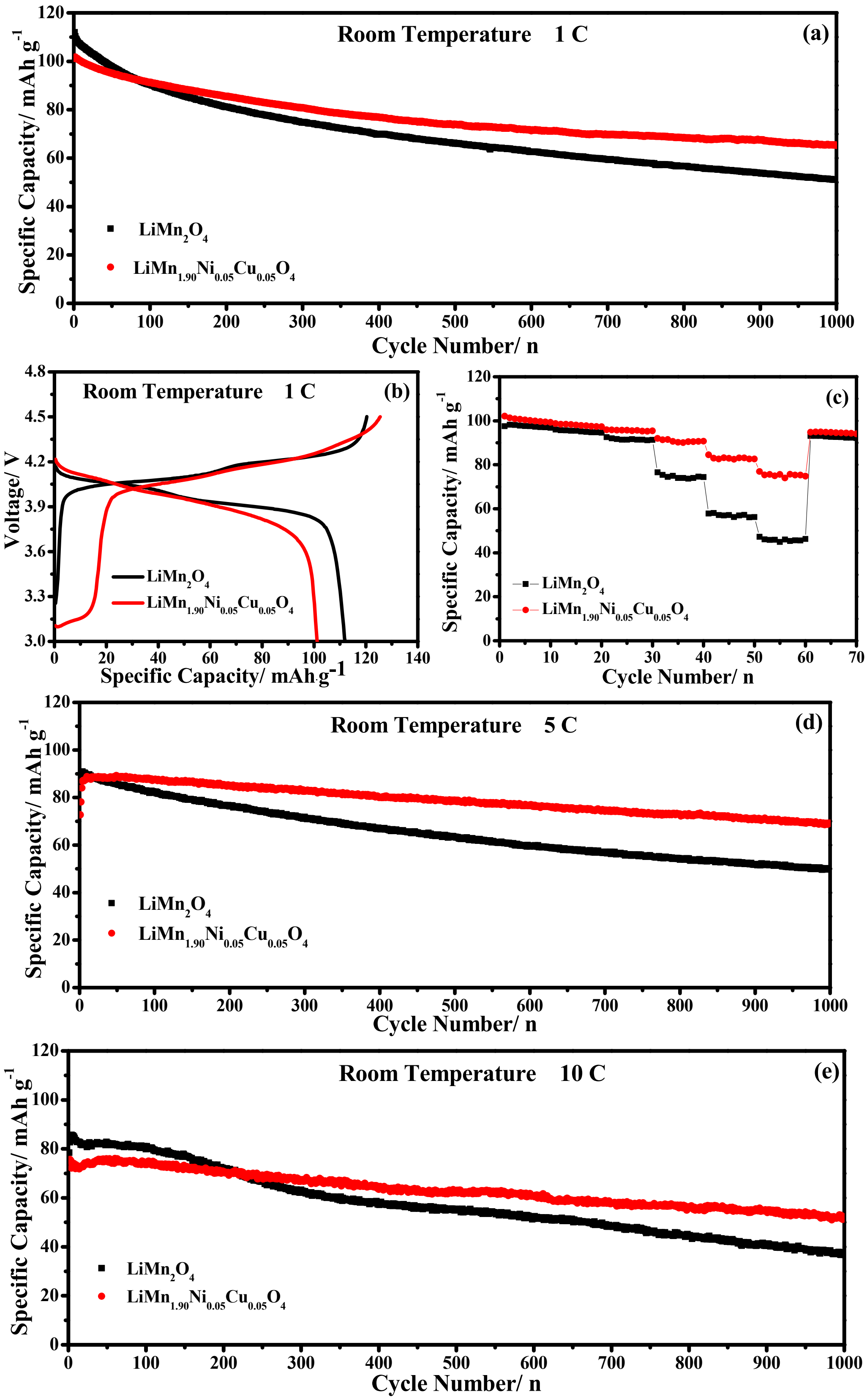

Figure 4. Cyclic performance diagram of $LiMn_2O_4$ and $LiMn_{1.90}Ni_{0.05}Cu_{0.05}O_4$ at (a) room temperature 1 C and (b) first charge discharge curve; (c) Multiplication performance diagram; (d) Cycle performance diagram at 5 C and (e) 10 C;

Figure4 (a). Cycle performance curves at 1 *C* and room temperature, (b) first charge-discharge curves, (c) rate performance curves, (d) long-cycle curves at 5 *C* and (e) 10 *C* for $LiMn_2O_4$ and (b) $LiMn_{1.90}Ni_{0.05}Cu_{0.05}O_4$

Figure 4 (a) shows the cycle curve of $LiMn_2O_4$ and $LiMn_{1.90}Ni_{0.05}Cu_{0.05}O_4$ after 1000 charges and discharges at room temperature 1 C. Figure 4 (b) is the corresponding first charge and discharge curve. It can be seen from Figure 4 (b) that the first charge discharge curves of the two samples at 3.9/4.1 V and 4.1/4.2 V both show two charge discharge plaorms for the two-step de intercalation reversible reaction with Li(32), indicating that Ni Cu co doping does not change the charge discharge mechanism of the initial spinel lithium manganate(79). The first discharge specific capacities of $LiMn_2O_4$ and $LiMn_{1.90}Ni_{0.05}Cu_{0.05}O_4$ at room temperature 1 C are 112.0 and 101.2 mAh g^{-1}, respectively. The first discharge specific capacities of $LiMn_{1.90}Ni_{0.05}Cu_{0.05}O_4$ are slightly smaller than that of $LiMn_2O_4$ because Ni Cu co doping replaces part of the active Mn^{3+} ions [19-20] for 1000 cycles. $LiMn_{1.90}Ni_{0.05}Cu_{0.05}O_4$ releases 51.0 and 65.3 mAh g^{-1} respectively, and the corresponding retention rates are 45.54% and 64.53% respectively.

Figure 4 (c) shows the magnification performance diagram of $LiMn_2O_4$ and $LiMn_{1.90}Ni_{0.05}Cu_{0.05}O_4$ at current densities of 0.5, 1, 2, 5, 8, and 10 C respectively. It can be seen that the discharge specific capacities of the two samples at 0.5 C are 97.5 and 102.1 mAh g^{-1} respectively. With the increase of current density, the specific capacities tend to decrease, This is because the polarization of the battery increases with the increase of current density [21] . At high current density of 5, 8 and 10 C, the discharge specific capacity gap between $LiMn_2O_4$ and $LiMn_{1.90}Ni_{0.05}Cu_{0.05}O_4$ gradually increases. At 10 C, $LiMn_2O_4$ and $LiMn_{1.90}Ni_{0.05}Cu_{0.05}O_4$ transport 47.2 mAh g^{-1} and 76.9 mAh g^{-1} respectively.

Figure 4 (d) and (e) show the cyclic curves of $LiMn_2O_4$ and $LiMn_{1.90}Ni_{0.05}Cu_{0.05}O_4$ at room temperature of 5 C and 10 C for up to 1000 times respectively. At 5 C, the initial discharge specific capacities of $LiMn_2O_4$ and $LiMn_{1.90}Ni_{0.05}Cu_{0.05}O_4$ are 89.7 and 86.9 mAh g^{-1} respectively. After 1000 cycles, the corresponding capacity retention rates are 55.74% and 79.52%, respectively. At 10 C, the initial discharge specific capacity of $LiMn_2O_4$ is 82.7 mAh g^{-1}, slightly higher than 75.0 mAh g^{-1} of $LiMn_{1.90}Ni_{0.05}Cu_{0.05}O_4$. However, after 1000 cycles, the specific discharge capacity of $LiMn_2O_4$ is only 36.7 mAh g^{-1}, and the retention rate is 44.38%. However, $LiMn_{1.90}Ni_{0.05}Cu_{0.05}O_4$ released 52.1 mAh g^{-1} after 1000 cycles, and the retention rate was as high as 69.47%.

3.5. AC impedance (EIS) test

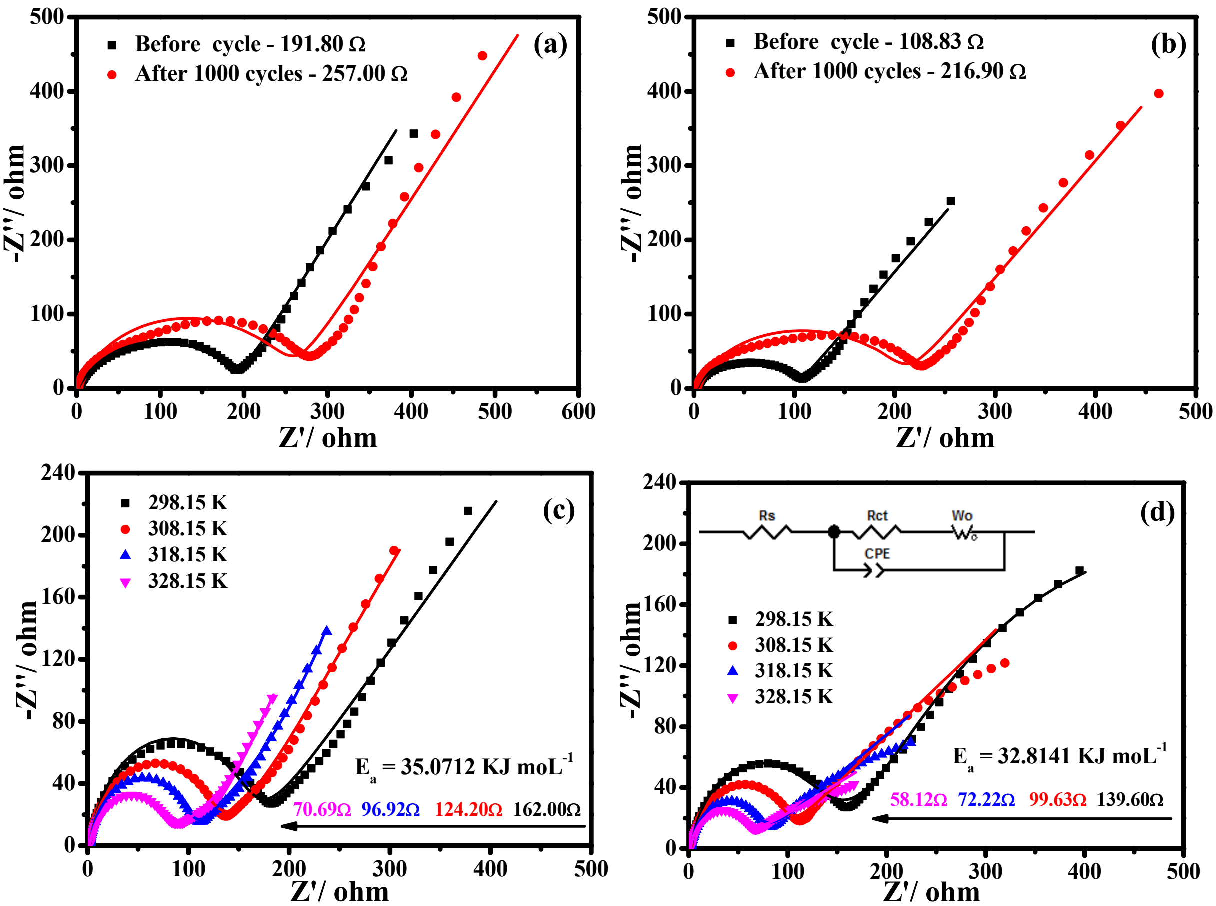

Figure 5. EIS diagram of (a) $LiMn_2O_4$ and (b) $LiMn_{1.90}Ni_{0.05}Cu_{0.05}O_4$ before and after 1000 cycles at 1 C at room temperature; (c) Activation energy curve of $LiMn_2O_4$ and (b) $LiMn_{1.90}Ni_{0.05}Cu_{0.05}O_4$;

Figure 5. EIS curves of (a) $LiMn_2O_4$ and (b) $LiMn_{1.90}Ni_{0.05}Cu_{0.05}O_4$ at before and after 1000 cycles under room temperature; activation energy curves of (c) $LiMn_2O_4$ and (b) $LiMn_{1.90}Ni_{0.05}Cu_{0.05}O_4$;

Figure 5 (a) and (b) show the EIS curves obtained before and after 1000 cycles at room temperature of 1 C for $LiMn_2O_4$ and $LiMn_{1.90}Ni_{0.05}Cu_{0.05}O_4$ respectively. It can be seen that the EIS curves of the two samples are composed of a flat semicircle formed by overlapping two semicircles from high frequency region to medium frequency region and a diagonal line in low frequency region [22-23] . Its corresponding equivalent analog circuit is shown in Figure 5 (d), where Rs represents solution resistance/ohmic resistance, Rct represents charge transfer resistance, CPE represents electric double layer capacitance, W0 represents Warburg impedance, reflecting the diffusion process of Li^+ [24]. By fitting $LiMn_2O_4$ and $LiMn_{1.90}Ni_{0.05}Cu_{0.05}O_4$, the Rct values of $LiMn_2O_4$ before and after 1000 cycles at room temperature 1 C are 191.80 and 257.00 Ω, respectively, which are greater than 108.83 and 216.90 Ω corresponding to $LiMn_{1.90}Ni_{0.05}Cu_{0.05}O_4$. In addition, the activation energy (Ea) test results of $LiMn_2O_4$ and $LiMn_{1.90}Ni_{0.05}Cu_{0.05}O_4$ at different temperatures (298.15 K, 308.15 K, 318.15 K and 328.15 K) are shown in Figure 5 (b) and (c). Respectively fitting, the Rct values of $LiMn_2O_4$ are 162.00, 124.20, 96.92 and 70.69 Ω, respectively, while the Rct values of $LiMn_{1.90}Ni_{0.05}Cu_{0.05}O_4$ are 139.60, 99.63, 72.22 and 58.12 Ω, respectively. It can be seen that the Rct value of $LiMn_{1.90}Ni_{0.05}Cu_{0.05}O_4$ at each temperature is slightly less than that of $LiMn_2O_4$. According to the equation:

$$lnR_{ct} = (E_a/R)T^{-1} + ln(RT/nFA)$$

In the formula, R is the gas constant (=8.314 J mol-1K $^{-1}$, F is the Faraday constant (=96485 C mol $^{-1}$, T is the thermodynamic temperature, A is the temperature coefficient, and n is the electron transfer number. After calculation, the Ea values of $LiMn_2O_4$ and $LiMn_{1.90}Ni_{0.05}Cu_{0.05}O_4$ are 35.0782 kJ mol $^{-1}$ and 32.8141 kJ mol $^{-1}$, respectively. $LiMn_{1.90}Ni_{0.05}Cu_{0.05}O_4$ shows good Li^+ diffusion rate performance.

3.6. Cyclic Volt Ampere (CV) Test

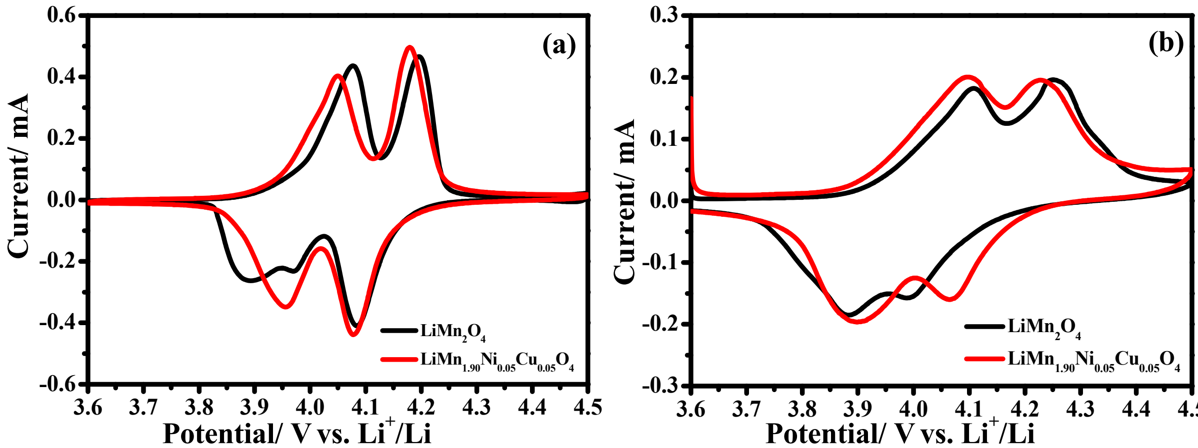

Figure 6. CV curves of $LiMn_2O_4$ and $LiMn_{1.90}Ni_{0.05}Cu_{0.05}O_4$ before (a) cycle and after (b) 1000 cycles at 1 C respectively;
Figure 6. CV curves of $LiMn_2O_4$ and $LiMn_{1.90}Ni_{0.05}Cu_{0.05}O_4$ at (a) before and (b) after 1000 cycles under 1 *C*;

Figure 6 (a) and (b) show the CV curves of $LiMn_2O_4$ and $LiMn_{1.90}Ni_{0.05}Cu_{0.05}O_4$ before and after 1000 cycles at room temperature of 1 C. It can be seen from the figure that the cycle curves of the two samples show two pairs of redox peaks around 4.05/3.95 V and 4.20/4.10 V before and after the cycle, which corresponds to the two plaorms on the first charge discharge curve in Figure 4 (b), indicating that Ni Cu co doping does not change the two-step stripping and embedding mechanism of Li(32)in the cycle(96). In Figure 6 (a), compared with $LiMn_2O_4$, the two pairs of oxidation peaks of $LiMn_{1.90}Ni_{0.05}Cu_{0.05}O_4$ shifted to the direction of low potential, which helps reduce electrode polarization, meaning that $LiMn_{1.90}Ni_{0.05}Cu_{0.05}O_4$ will have better electrochemical reversibility. After 1000 cycles, $LiMn_{1.90}Ni_{0.05}Cu_{0.05}O_4$ retains larger peak area and smaller potential difference, which also indicates the excellent reversibility during the cycle.

4. Conclusion

In this paper, spinel $LiMn_2O_4$ and $LiMn_{1.90}Ni_{0.05}Cu_{0.05}O_4$ cathode materials were successfully prepared by solution combustion method. Ni Cu co doping effectively reduces the particle size and improves the crystallinity of the material. At room temperature of 1 C, $LiMn_{1.90}Ni_{0.05}Cu_{0.05}O_4$ obtained an initial discharge specific capacity of 101.2 mAh g $^{-1}$ and retained 64.53% after 1000 long cycles, while only 45.54% of $LiMn_2O_4$ was obtained under this condition. At high current of 5 C and 10 C, $LiMn_{1.90}Ni_{0.05}Cu_{0.05}O_4$ also obtained high discharge specific capacity and capacity retention rate, showing excellent rate performance. CV and EIS tests also further proved that $LiMn_{1.90}Ni_{0.05}Cu_{0.05}O_4$ has a small electrode polarization and electrochemical reversibility, and shows a low charge transfer resistance and redox potential difference before and after 1000 cycles. The activation energy test results show that the Ea value of $LiMn_{1.90}Ni_{0.05}Cu_{0.05}O_4$ is 32.8141 kJ mol $^{-1}$, slightly lower than the 35.0782 kJ mol $^{-1}$ of $LiMn_2O_4$, indicating that it has an excellent diffusion rate of Li^+.

Acknowledgments

Fund project: Pu'er University Innovation Team Project (CXTD014)

References

[1] Wu, H. M.; Tu, J. P.; Chen, X. T.; et al. J Solid State Electer. 2007, 11(2):173-176. DOI: 10.1007/s10008-005-0082-y.

[2] Wang, F. X.; Xiao, S. Y.; Shi, Y.; et al. Electrochimica Acta. 2013, 93:301-306. DOI: 10.1016/j.electacta.2013.01.106.

[3] Cui, P.; Liang, Y. Solid State Ionics, 2013, 249-250:129-133. DOI: 10.1016/j.ssi.2013.08.002.

[4] Hendriks, R.; Cunha, D. M.; Singh, D. P.; et al. ACS Appl Energ Mater, 2018, 1(12). DOI: 10.1021/acsaem.8b01477.

[5] Hai-Lang, Z.; Ren, R.; Jing, A. Materials Science Forum. 2011, 686:716-719. DOI: 10.4028/www.scientific.net/MSF.686.716.

[6] Marinca, A. H.; Goga, F.; Dorneanu, S. A.; et al. J Solid Electr, 2020, 24(3):473-497. DOI: 10.1007/s10008-019-04467-3.

[7] Jiang, J.; Gong, G.; Li, C.; et al. Nanosci Nanotech Let. 2017, 9(5):668-672. DOI: info:doi/10.1166/nnl.2017.2372.

[8] Xion, L. L.; Zhang, C.; Tao, T.; et al. Acta Phys. – Chim. 2012, 28(5):1177-1182. [Xiong Lilong, Zhang Cheng, Tao Tao, et al. Journal of Physical Chemistry, 2012, 28 (5): 1177-1182.] DOI: 10.3866/PKU WHXB201203092.

[9] Gao, X.; Ikuhara, Y. H.; Fisher, C. A. J.; et al. J Mater Chem A. 2018, 7, 20-27. DOI: 10.1039/C8TA08083F.

[10] Qiu, X. Y.; Zhuang, Q. C.; Wang, H. M.; et al. Acta Phys. – Chim. 2010(06):1499-1506. [Qiu Xiangyun, Zhuang Quanchao, Wang Hongming, et al. Journal of Physical Chemistry, 2010 (06): 1499-1506.] DOI: 10.3866/PKU WHXB20100608.

[11] Wang, H.; Zeng, Y.; Huang, K.; et al. Electrochim Acta. 2007, 52(15):5102-5107. DOI: 10.1016/j.electacta.2007.02.004.

[12] Waller, G. H.; Brooke, P. D.; Rainwater, B. H.; et al. Journal of Power Sources, 2016, 306(feb.29):162-170.DOI:10.1016/j.jpowsour.2015.11.114.

[13] Zhu, J. Y.; Liu, Q.; Xiang, M. W.; et al. Modern Chemical Industry. 2020, 40(5):104-108. [Zhu Jinyu, Liu Qing, Xiang Mingwu, et al. Modern Chemical Industry, 2020, 40 (5): 104-108.] DOI: 10.16606/j.cnki.issn0253-4320.2020.05.024

[14] Zhang, C. L.; Wang, W. J.; Zhang, J.; et al. Acta Phys. – Chim. 2008, 23. [Zhang Chunling, Jiang Weijun, Zhang Jing, et al. Journal of Physical Chemistry, 2008, 23.] DOI: 10.3866/PKU WHXB2007Supp08.

[15] Amarilla, J. M.; Petrov, K.; Pico, F.; et al. J Power Sources. 2009, 191(2):591-600. DOI: 10.1016/j.jpowsour.2009.02.026.

[16] Xion, L. L.; Zhang, C.; Tao, T.; et al. Acta Phys. – Chim. 2013, 29(04):763-769. [Xiong Lilong, Xu Youlong, Tao Tao. Journal of Physical Chemistry, 2013, 29 (04): 763-769.] DOI: 10.3866/PKU WHXB201302211.

[17] Wei, Y.; Nam, K. W.; Kim, K. B.; et al. Solid State Ionics. 2006, 177(1-2):29-35. DOI: 10.1016/j.ssi.2005.10.015.

[18] Chen, L.; Zhai, W.; Chen, L.; et al. Journal of Power Sources, 2018, 392:116-122. DOI:10.1016/j.jpowsour.2018.04.103.

[19] Deng, J.; Xu, Y.; Xiong, L.; et al. J Alloy Compd. 2016, 677:18-26. DOI: 10.1016/j.jallcom.2016.03.256.

[20] Shuo, Y.; Dirk, S.; Abhishek, K.; et al. Materials, 2018, 11(5):806. DOI：10.3390/ma11050806.

[21] Wang, S. M.; Liu, H. L.; Xiang, M. W.; et al. New J Chem. 2020, 44(25):1-10. DOI: 10.1039/D0NJ01290D.

[22] Yair, E. E.; John, T.; V.; Michael, M. T.; et al. [J]. Cheminform. 2010, 30(24):908-913. DOI: 10.1002/chin.199924014.

[23] Jiang, C.; Tang, Z.; Wang, S.; et al. Journal of Power Sources, 2017, 357(Jul.31):144-148. DOI:10.1016/j.jpowsour.2017.04.079.

[24] Iqbal, A.; Int. J. Electrochem. Sci. 2019, 14, 929-942. DOI: 10.20964/2019.01.79.

[25] Ebin, B.; Sebahattin, G.; Lindbergh, G. Ceram Int. 2014, 40(1):1019-1027. DOI: 10.1016/j.ceramint.2013.06.099.

[26] Ohashi,T; Ken-ichi O; Fukunaga, T.; et al. ChemElectroChem. 2020, 7(7):1644–1651. DOI: 10.1002/celc.202000173.

[27] Fang, T. T; Chung, H. Y. Electrochem Solid ST. 2011, 14(4):A49. DOI: 10.1149/1.3541055.

[28] Yang, M. C.; Xu, B; Cheng, J. H.; et al. Chemistry of Materials, 2011, 23(11):2832-2841. DOI: 10.1021/cm200042z.